Journal of Applied Catalysis and Engineering

https://doi.org/10.17756/acce.2020-004

Research Article

Open Access

Influence of Selective Deposition of CeO_2 and CuO on Surface MWCNTs Walls on the Activity, Selectivity and Stability in the PROX Reaction

Dayana Sánchez[1], Amanda Garcez[2], Fabio Souza Toniolo[3] and Martin Schmal[1, 3*]

[1]*Department of Nanotechnology Engineering, PENt, COPPE, Federal University of Rio de Janeiro, Brazil*

[2]*Laboratory for X-Ray Photoelectron Spectroscopy, Department of Physical Chemistry, Federal University of Rio de Janeiro, Brazil*

[3]*Chemical Engineering Program of COPPE/UFRJ, Federal University of Rio de Janeiro, Brazil*

***Correspondence to:**
Chemical Engineering Program of COPPE/UFRJ
Federal University of Rio de Janeiro
P.O. BOX 68502, CEP 21941-914
Rio de Janeiro/RJ, Brazil.
Tel: +55 21 3938-8352
E-mail: schmal@peq.coppe.ufrj.br

Received: December 22, 2020
Accepted: January 04, 2021
Published: January 06, 2021

Citation: Sánchez D, Garcez A, Toniolo FS, Schmal M. 2020. Influence of Selective Deposition of CeO_2 and CuO on Surface MWCNTs Walls on the Activity, Selectivity and Stability in the PROX Reaction. *J Appl Cat Chem Eng* 1(1): 17-28.

Published by United Scientific Group

Abstract

In the present study, we synthesized catalysts based on CuO_2 and CeO_2 on pretreated MWCNT (Multi-Walled Carbon Nanotubes) support. The metallic oxides were selectively deposited (on internal and/or external surfaces of the MWCNT) by wet impregnation. The CeO_2/CNT@CuO, CuO/CNT@CeO_2 and CuO-CeO_2/CNT@CeO_2 catalysts (which means "external component"/CNT@"internal component") were tested in the PROX reaction. We studied the selective introduction of the CuO and CeO_2 nanostructures in and outside the CNT (carbon nanotubes) walls and their influence on the activity, selectivity and stability in the PROX reaction. Characterizations showed that it was possible to drive selectively the deposition of the metallic oxides to one of the MWCNTs surface. Results showed that the activity does not depend whether metallic oxides are internally or externally located on the MWCNTs walls. There are no sintering or interaction of metal oxides. The catalysts reached high conversions 65-70% and are very stable for long time. The CNT contribute to the electronic mobility of the electrons of metal oxide and the CNTs.

Keywords

MWCNT, Selective deposition, Metal oxides, CO oxidation, Activity, Stability

Abbreviations

PROX: Preferential Oxidation of a Carbon Monoxide; MWCNT: Multi-Walled Carbon Nanotubes; CNT: Carbon Nanotubes

Introduction

The preferential CO oxidation is widely used for treating H_2-rich streams for use in fuel cells [1, 2]. The noble metals have been used for PROX reaction, at low temperatures, however, they are expensive [3-6]. The transition metals and oxides present high performance and enormous potential. The catalytic activity of the oxidation reaction depends on several factors. Among these, the support materials such as silica, alumina, carbon, among others, show a dominant influence on the catalytic performance [7, 10, 13]. Indeed, noble metals and nickel oxide are excellent activation metal oxides for this reaction, but the first is very expensive while nickel oxide is very susceptible to quick deactivation, which is disadvantageous for this reaction. On the other hand, the oxide supports have been vastly cited in the literature and although they show stable performance,

there are disadvantages due to sintering and formation of byproducts, due to the different surface properties of the supports. Therefore, according to the literature, the cerium oxide (CeO_2) and copper oxide (CuO) have been excellent active oxides when supported on oxide or mixed oxide supports for this reaction [7]. In fact, the CeO_2 presents vacancies and high storage capacity, which contributes to the redox processes. The interaction between redox ion pairs gives rise to the interface CuO-CeO_2. Martinez-Arias [8] showed that the CO adsorption and subsequent CO_2 formation takes place at this interface on CuO/CeO_2 and CuO/$ZrCeO_4$ catalysts. Zhu [9] also prepared CuO-CeO_2 mixed oxide catalysts by the hydrothermal method, varying the composition, and showed that the CuO concentration influenced the activity. The CO conversions are high, which were ascribed to the synergistic effect between the Cu and Ce oxide particles and due to the high dispersion and homogeneity of the metallic oxide distribution in accordance with other results [10-12].

Since the support affects the reaction performance and the stability, the literature began to search for new materials that may inhibit sintering and/or interaction with the active metallic oxides during the oxidation reaction and in particular for the PROX reaction. Among them, the carbon nanotubes provide an innovative and interesting approach by giving a nano-confined environment (empty internal surface). Besides, the nanotubes contribute to a higher exposition of the metals or oxides, good stability and longer lifetimes. Moreover, the nanotubes intervene in the electronic structure of the metal or oxide and influence the adsorption and diffusion of reagents and products [12, 14, 15]. The MWCNTs have major advantages because they are inert, avoid sintering or interactions with the active metal oxides, and the oxides can be regenerated.

However, for CNT there are two issues: (i) the access to the internal surface while controlling and driving the deposition of the metallic oxides to one of the surfaces (internal or external), which is important for synthesizing bifunctional catalysts; (ii) it is very important to verify the dispersion of such active sites on the inner and outer walls of the CNT. How and whether the location of the active sites influences the reaction rate or the catalytic activity occurring on the internal or external walls of the CNT, or if instead, the location of these metal oxide does not influence the activity of the catalysts. The literature is scarce concerning the use of CNT in catalysis, the metal distribution on CNT surface walls, the metal concentration, metal deposition on inner and outer walls, and mainly how this deposition influences the reaction. Due to the high surface area, the dispersion of metal and metal oxide is much higher than on oxide supports. The high surface area facilitates the dispersion of metals, increasing the activity. Wang et al. [16] were the first authors who introduced Pt nanoparticles in MWCNTs deposited preferably on the internal surface wall of the carbon nanotubes. Tessonier [17] used an organic solvent to deposit Pt nanoparticles. The organic solvents in contact with the external surface easily reach the inner walls and due to the low surface tension allow higher control during the deposition of the particles. Astinchap [18] suggested a different method, in which the internal surface containing the nanoparticles previously deposited was protected using an organic solvent. Ma [19] obtained NiO nanoparticles deposited on the external and internal surface for the dry reforming of methane. Kozonoe [60] introduced Fe-Co-Cu oxide and NiO selectively on the inner and outer walls of the MWCNTs walls for the methane reforming.

Here, we chose CuO and CeO_2 nanostructures, the first as active phase and the second as oxygen storage supplier, both introduced selectively and alternatively on the inner and outer walls of MWCNT or both on the outer wall to study the influence of the location of each oxide on the activity and stability of the catalyst in the PROX reaction. We used organic solvents for the selective addition of metal in and out of the CNT, and performing complete characterizations we verified the effectiveness of selective deposition. Then, using the PROX reaction as a test, we verified the influence of the location of these oxide nanostructures at the MWCNTs walls on the conversion and reaction rates, the influence of the metal oxide concentration on the activity and finally the stability of the catalysts and the effects on their surface after catalytic evaluation.

Experimental Section

We synthesized catalysts meaning "external component"/CNT@"internal component", or specifically CeO_2/CNT@CuO, CuO/CNT@CeO_2, and CuO-CeO_2/CNT@CeO_2 catalysts, in the last one both phases are settled externally (bimetallic), using precursor solutions of $Cu(NO_3)_2{\cdot}_3H_2O$ and $Ce(NO_3)_3{\cdot}_6H_2O$. The nanotubes were supplied by the UFMG, Brazil and were synthesized by the CVD method (commercial). Throughout this paper, CNT is a codification for multi-wall carbon nanotubes (MWCNT). The proposed methodology was divided into three stages: (i) functionalization of carbon nanotubes (MWCNT); (ii) deposition of nanoparticles (CeO_2 or CuO) on the internal surface of the functionalized MWCNT; (iii) and finally deposition of nanoparticles (CeO_2 or CuO) on the external surface of MWCNT, with the nanoparticles previously inserted on the internal surface. The total concentration was 10 wt. %, or 5 wt. % for CeO_2 and 5 wt. % for CuO. For the bimetallic catalyst, the total loading on the external surface was 5 wt. % or 2.5 wt. % of CeO_2 and 2.5 wt. % CuO, as presented in table 1. Codification meaning "MeOe"-CNT@"MeOi".

Table 1: Specifications of the catalysts. Location of the metallic oxides and loading (%) of the oxides on internal and external surfaces of the MWCNT.

Catalysts	Internal Surface	External Surface
CeO_2/CNT@CuO	5% CuO	5% CeO_2
CuO/CNT@CeO_2	5% CeO_2	5% CuO
CuO-CeO_2/CNT@CeO_2	5% CeO_2	2.5% CuO; 2.5% CeO_2

Functionalization of carbon nanotubes

The raw carbon nanotubes were functionalized with HNO_3 (65% by mass) at 140 °C for 16 h. We used a mass/volume ratio of 10 g of CNTs for each 500 mL of HNO_3 (65%). Magnetic stirring was maintained during the oxidative treatment. Then,

the solid was filtered, washed several times with deionized water (until reaching pH 7) and dried at 100 °C for 12 h.

Deposition of metallic oxides on the inner wall of the CNT

The CeO_2 and CuO were introduced selectively by wet impregnation in the functionalized MWCNT on the inner and outer walls, as "external component"/CNT@"internal component". We prepared three samples: CeO_2/CNT@CuO, CuO/CNT@CeO_2 and CuO-CeO_2/CNT@CeO_2 catalysts. After functionalization, the total pore volume of the nanotubes was 0.6 g/cm^3. Ethanol solution smaller or equal to the total pore volume was used to deposit the metal oxide on the inner surface wall of the nanotubes. The precursor solution (Cu or Ce) in ethanol (0.4 mL) was slowly added to the functionalized carbon nanotubes (2 g) and an equal volume of distilled water was added (0.4 mL). Once the wet point was reached, the materials were dried in the muffle furnace at 100 °C for 1 h. This procedure was repeated several times until the total volume of the precursor solution was completed. Then, the impregnated nanotubes were dried at 100 °C for 12 h. Subsequently, the material was washed with deionized water to clean the external surface of the CNTs. The internal surface along with the deposited nanoparticles was protected by adding 1 mL of benzene and then washed for removing the nanoparticles on the outer surface. Finally, the solid was dried at 100 °C for 12 h. The samples obtained in the first step of preparation were assigned as CNT@CuO, CNT@CeO_2, and CNT@CeO_2 (@internal component). Different from the methodology described elsewhere [18], our materials were not calcined and not re-functionalized.

Deposition of metallic oxides on the outer wall surface

Of the samples prepared previously, CNT@CuO, CNT@CeO_2, and CNT@CeO_2 was performed by adding aqueous solutions of the corresponding precursors of Cu and Ce nitrates. In this stage, the internal surface was previously protected with 1 mL benzene. Benzene penetrates and fills the inner walls of the nanotubes. Thereafter, the precursor solutions of the metal oxide nitrates were impregnated and adhered to the outer walls by anchoring over the surface of carbon nanotubes. These samples were dried at 100 °C for 12 h and finally calcined under N2 flow at 60 mL/min and 400 °C (10 °C/min) for 2 h. The final catalysts were codified as CeO_2/CNT@CuO, CuO/CNT@CeO_2 and CuO-CeO_2/CNT@CeO_2. ("external component"/CNT@"internal component").

Characterizations

X-ray diffraction

The crystalline phases of the catalysts were studied in a Miniflex Rigaku diffractometer with Cu/Kα radiation (λ = 1.5418Å) operated at 30 kV and 15 mA. Data acquisition was done in the range of 10° ≤ 2Θ ≤ 90°, semi-continuous mode, and scanner speed of 0.05°/s.

Raman spectroscopy

It was used to identify the structural properties of the catalysts and was performed at room temperature on a LabRam HR-UV800/Jobin-Yvon spectrometer, 1 μm^3 resolution and equipped with an Olympus BX41 microscope, a thermal conductivity detector, operated at -70 °C, a He-Ne laser (λ = 632 nm) and "spot" of 100 μm size.

X-Ray photoelectron spectroscopy

The external surface of the catalysts was studied using X-ray photoelectron spectroscopy (XPS). The powder samples were analyzed in a Thermo Scientific (ESCALAB 250Xi) brand equipment. The sample was placed in an ultra-high vacuum chamber below 10-7. The x-ray source was (Al-Kα) with monochromatic light (hv = 1486.6 eV) in CAE (Constant Energy Analyzer) mode, 100 eV pass-through energy for survey and 25 eV for high resolution. The spectrometer was calibrated with copper patterns. The standard carbon line (C1s) at 283.4 eV was used as a calibration reference.

Transmission Electron Microscopy

The ultra-high microscopy analysis was performed in an FEI Titan 80-200 apparatus equipped with BrukerChem STEM EDS system for obtaining the images of the metal oxide on the surface of the CNT. 1 mg of powder sample was suspended in ethanol and dispersed by using ultrasound for 20 min. A drop of the solution was suspended on a copper grid coated with a carbon film (lacey carbon), 400 mesh and Formvar coating. The grid was dried at room temperature.

Catalytic tests

Catalytic evaluation of the catalysts was carried out in a bench unit containing a U-shaped Pyrex glass reactor, a furnace, a thermocouple Therma model TH 90DP, coupled to a gas chromatograph. Gas compounds were analyzed in a Shimadzu GC-2014 chromatograph with two thermal conductivity detectors (TCD) and two chromatographic columns to separate O_2, N_2, CO, H_2, H_2O, CO_2. The concentration of the monitored gas compounds was calculated based on the calibration of standard gas mixtures in known quantities of products and reagents. For the catalytic tests, a mass of 100 mg of the catalyst was pretreated in situ in pure H_2 flow (60 mL.min-1) at 450 °C for 1 h (10 °C.min^{-1}).

Subsequently, the reactor was cooled down to room temperature under N_2 flow. Then, the catalyst was exposed to the mixture of 2% CO, 2% O_2, 54.7% H_2, 10% N_2 (internal standard), and He balance. The total flow was maintained at 100 mL.min^{-1} during the tests. The catalysts were evaluated at temperatures of 150, 180 and 200 °C, returning and remaining at 180 °C for 20 h, with GC injections every 1.5 h. The CO conversion (XCO), O_2 conversion (XO_2), CO_2 selectivity (SCO_2) and the rates of reaction were calculated according to Equations (1), (2), (3) and (4).

$$X_{CO} = ([CO]_{in} - [CO]_{out})/[CO]_{in} \times 100\% \quad (1)$$

$$S_{CO2} = 0.5([CO]_{in} - [CO]_{out})/([O2]_{in} - [O2]_{out}) \times 100\% \quad (2)$$

$$X_{O2} = ([O2]_{in} - [O2]_{out})/[O2]_{in} \times 100\% \quad (3)$$

$$Rate = ([F]_{in} * X_{CO})/m_{cat}\ (mol.g^{-1}.min^{-1}) \quad (4)$$

Results and Discussion

XRD analyses

The raw and the functionalized carbon nanotubes (CNT) and the catalysts were analyzed by XRD (Figure 1). The diffraction patterns of CAT A, CAT B, and CAT C catalysts are shown in figure 1.

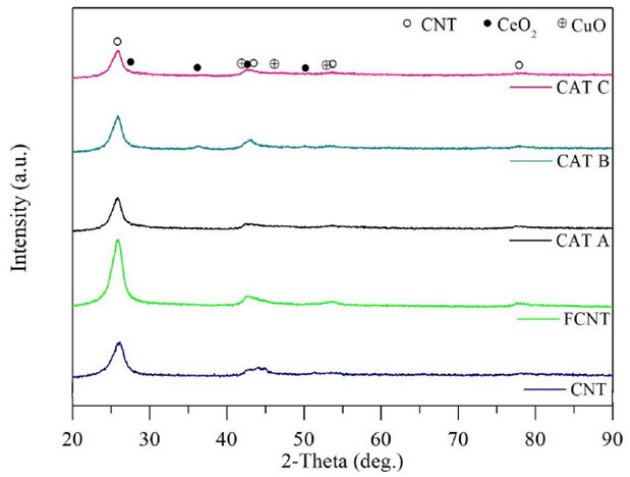

Figure 1: XRD patterns of CNT, FCNT, CeO_2/CNT@CuO (CAT A), CuO/CNT@CeO_2 (CAT B) and CuO-CeO_2/CNT@CeO_2 (CAT C) catalysts.

The diffractograms show one intense peak at 2Θ equal 26°. The peak associated with the crystallographic plane (0 0 2) is characteristic of the reflection of the carbon structure. Also, another peak was observed with lower intensity at 2Θ = 43° that corresponds to the diffraction plane (1 0 0). These peaks are characteristic of hexagonal graphite [21-23]. The diffraction peaks of CAT A (CeO_2/CNT@CuO), CAT B (CuO/CNT@CeO_2) and CAT C (CuO-CeO_2/CNT@CeO_2) indicate the presence of the metallic oxides on the surface of the nanotubes at 35.5°, 42.25°, 46.16° and 53.32° identified for CuO phase (PDF#440706) [24]. The peaks at 27.32°, 36.71°, 42.04° and 50.62° are characteristic of the cerium oxide (CeO_2) with hexagonal structure (PDF#44-1001) [12]. The CAT A displays more intense peaks of the copper oxide phase compared to the CeO_2 peaks, probably because of the higher concentration of the CuO on the surface. On the other hand, the peak intensity of the CeO_2 phase present on the outer walls of the CNT is lower. The diffractogram of CAT B displays more intense peaks, associated with CeO_2, ascribed to the higher concentration of CeO_2 on the internal surface. The environment favored the reduction of the Ce precursor, decreasing the reduction temperature since it was possible to consolidate the CeO_2 phase more easily. Similar behavior was observed for CAT C. Peaks of the CeO_2 phase were more intense compared with the peaks of the CuO phase. Oxidation of the cerium precursor took place to a higher extent. The lower intensity of the CuO diffraction peaks indicates well-dispersed species on the surface of the CNT, also on the CeO_2, due to the lower concentrations that were not detected by the XRD analysis.

Raman spectroscopy

Structural properties of the catalysts were also studied by Raman spectroscopy. The materials evaluated between 900-1800 cm^{-1} showed the bands D, G, and D′ (Figure 2). The D-band observed at 1335 cm^{-1} was related to amorphous and disordered carbon that evidences structural defects, such as vacancy, heptagon-pentagon pairs, bifurcations, openings and curvatures. The G band located around 1585 cm^{-1} indicates the ordered graphite and is associated with the tangential vibration of carbon atoms [25]. The shoulder D′ at 1616 cm^{-1} stands out from the G band. This band is indicating the disordered carbon and defects in the graphite structure [26]. These results also suggest that the graphitic structure of the nanotubes is preserved after oxidative treatment with HNO_3 [27]. According to the literature, the low intensity of the bands may be related to the interference of the metallic oxides. The metals act as a load-donor system that intervenes in the vibration of vibrational modes. Polychronopoulou [28], Zedan [30] and Shi [11] observed signals in the regions between 200-500 cm^{-1} and 460-470 cm^{-1}, which are associated with copper oxides and cerium oxides, respectively, not observed here. In fact, the concentration of the metallic oxides is very low.

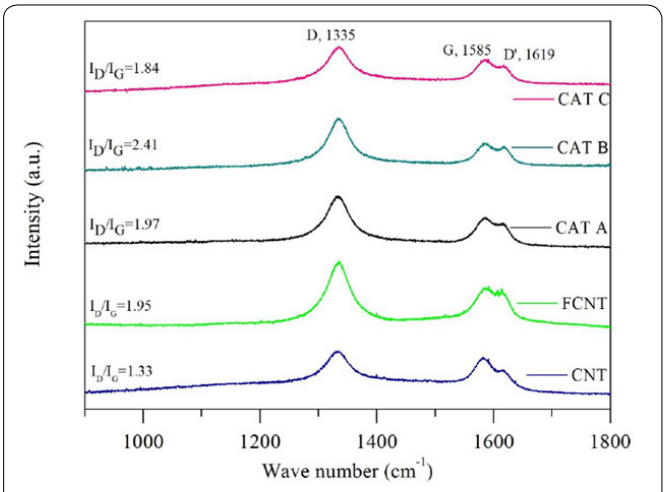

Figure 2: Raman spectra of CNT, FCNT, CeO_2/CNT@CuO (CAT A), CuO/CNT@CeO_2 (CAT B) and CuO-CeO_2/CNT@CeO_2 (CAT C) catalysts.

The ID/IG ratio indicates the degree of graphitization. High ID/IG ratios are associated with the formation of structural defects [31, 32]. Motchelaho [33] and other authors found that after the oxidative treatment, the ID/IG ratio is high indicating breakage of nanotubes, formation of defects and addition of functional groups. CAT A, CAT B and CAT C catalysts showed ID/IG ratios of 1.97, 2.41 and 1.84 respectively. These results indicate structural changes after the deposition of copper and cerium oxides. Ma [19] observed for nickel catalysts supported on carbon nanotubes that the ID/IG ratios changed depending on the location of the nanoparticles (internal or external surface of CNTs). Metal particles deposited externally did not show significant changes, which indicates that the nanoparticles deposited on the external surface have not modified the graphitic structure of the support. On the other hand, when the nanoparticles were deposited on the inner walls of the nanotubes, structural changes in the graphite layers were notorious, due to deep defects mostly disordered. Ma [19] showed that the

nanoparticles were deposited simultaneously on the inner and the outer surface of the nanotubes. High values of ID/IG ratio indicate a more disordered structure of the nanotubes [34, 35]. These results agree with the literature and indicate that metallic oxides were deposited on the inner and outer surface walls of the carbon nanotubes. In fact, nanoparticles were anchored on the defects and/or functional groups inserted during the functionalization of the nanotubes, which also suggest high dispersion of the metal oxides and strong interaction with the CNT.

TEM analyses

TEM images of CAT A and CAT B catalysts showed the opening of the tips of CNT, as well as the formation of defects as bifurcations and excessive curves, which confirms the effective functionalization process. The open ends facilitate the introduction of metallic oxides into the inner walls of the support. The internal and external diameters of the nanotubes are 6.9 and 8.9 nm, respectively. We identified 16 walls with layers spacing of 0.206 nm. These results were also observed in references [12] and [17] and are representative of the crystallographic plane (0 0 2) of the hexagonal graphite. For the CAT A catalyst, the images in figure 3 display nanoparticles with regular shapes and well dispersed on the internal and external surfaces of the nanotubes.

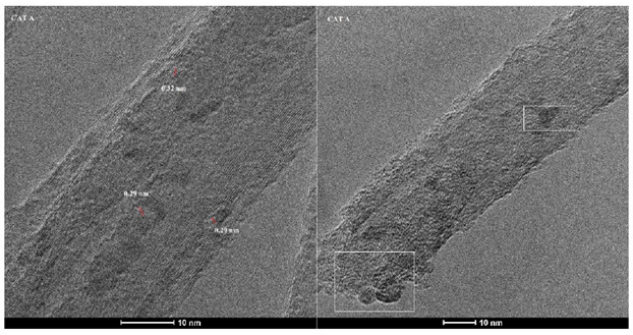

Figure 3: Images of Transmission Electron Microscopy (TEM) of CeO_2/CNT@CuO (CAT A) catalyst with identification of CeO_2 and CuO nanoparticles.

The nanoparticles on the inner wall of the nanotubes are oval-shaped particles with a mean diameter of 5.6 nm and interplanar distances of 0.29 nm. According to Shi [11], the nanoparticles are ascribed to the CuO phase. Authors associated these results with the crystallographic plane (110) of the CuO with spacing between planes of 0.267 nm. As well, the nanoparticles anchored on the external surface also showed regular spherical shapes. It was estimated an average diameter of 7.2 nm with crystalline planes spacing of 0.32 nm. Shi et al. [11] found that CeO_2 (111) presented spacing between planes of 0.31 nm. These results are consistent with our observations and confirm the formation of CuO and CeO_2.

Figure 4 shows TEM images of CAT B catalyst, which are similar to CAT A catalyst. The nanoparticles deposited probably on the internal surface have an average diameter of 3.7 nm and crystalline plane spacing of 0.32 nm (see details in Supplementary Material 3). The diameter of the nanoparticles deposited on the outer walls was 4.8 nm with a spacing of 0.27 nm. Based on these results, probably CeO_2 nanoparticles are deposited on internal walls and CuO decorates the external walls of carbon nanotubes. The small size of the nanoparticles suggests a good interaction between the inner surface and the metallic oxides. Also, the small sizes of the oxides deposited on the external surface may be related to electrostatic interactions between the oxides and the functional groups existing on this surface. This interaction favored the decrease in size and improved the dispersion of particles on the surface of catalysts [16].

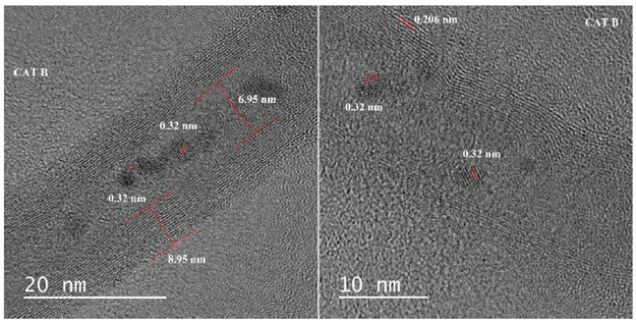

Figure 4: Images of Transmission Electron Microscopy (TEM) of CuO/CNT@CeO_2 (CAT B) catalyst with identification of CeO_2 and CuO nanoparticles.

According to the literature, when a solid solution is formed usually there is a crystal shrinkage phenomenon. The interplanar crystal spacing of CeO_2 in CAT A and CAT B catalysts does not exhibit shrinkage in comparison with values of pure CeO_2 (0.3124 nm) reported in the literature, indicating that a high percentage of the copper and cerium oxides in the CAT A and CAT B catalysts could be found isolated on the walls of the carbon nanotubes [12]. Also, the larger copper content (5 wt. % for CAT A and CAT B catalysts) could mainly lead to the presence of larger CuO particles, comparing with 2.5 wt. % CuO deposited on the CAT C catalyst (not shown). Also, for CAT C catalyst, copper and cerium were deposited simultaneously on the external surface of carbon nanotubes. The Cu^+ (74 pm) radius is smaller than Ce^{4+} one (92 pm), so it is likely that some of the copper tapped onto the ceria oxide or in the lattice [57-59].

XPS analyses

The XPS analyses were performed for identifying the oxidation state of copper and cerium oxides deposited on the outer surface of the CNT, and also identifying the functional groups of the functionalized MWCNTs. All binding energies were corrected referencing to the C1s (284.6 eV) peak of the contamination carbon as an internal standard. Results are shown in table 2.

Figure 5 shows the deconvolution of C1s peak. Results showed graphitic carbon at 284.3 eV [41]. The peak at 285.6 eV was related to defects in the lateral walls and tips of the carbon nanotubes [42, 43]. Peaks at 286.5, 288.5, 290.5, and 291.5 eV are assigned to the carbon atoms attached to groups containing oxygen in their structure [44]. The electronic transition of orbitals $\pi \rightarrow \pi^*$ was associated with the peak at 290.9 eV. These results indicate the functionalization of the external surface and also that the graphite layers retained their original structure [12].

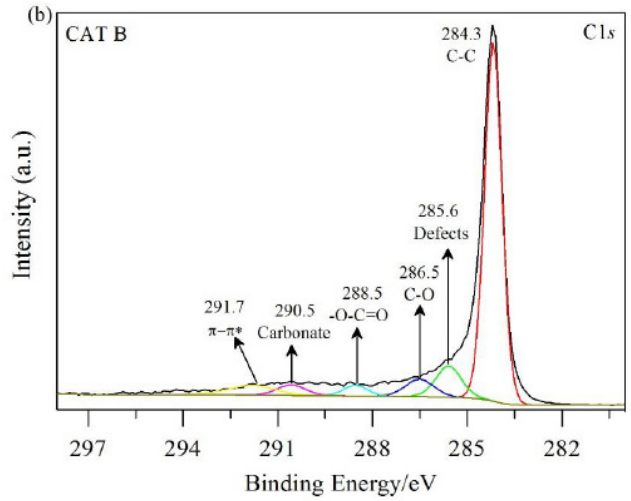

Figure 5: Peak deconvolution C1s of the (b) CuO/CNT@CeO_2 (CAT B) catalyst. The standard C1s line at 283 eV was used as calibration reference. Supplementary material 1: (a) CeO_2/CNT@CuO (CAT A) and (c) CuO-CeO_2/CNT@CeO_2 (CAT C) catalysts.

The deconvolution of the oxygen peaks is shown in Figure 6 and displays bands at 533.8 and 531.5 eV which are associated with carboxylic and hydroxyl groups, respectively. The peak at 530.5 eV was associated with oxygen adsorbed on the surface. These results corroborated the functionalization of the carbon nanotubes. The peaks at 529.3, 529.5, and 529.4 eV, respectively for CAT A, CAT B, and CAT C, are related to the metallic oxides on the external surface of the CNTs. These peaks were associated with oxygen from copper and cerium oxides. Additionally, CAT B shows two other peaks at 534.7 and 536.2 eV, and CAT C presents an additional peak at 535.5 eV, which may have a relationship with vacancies formed, sub-surfaces of CeO_2, evidencing the presence of Ce^{3+}species [45].

The oxygen peaks (O1s) of the CAT B and CAT C (Supplementary Material 1) show higher intensity at 529.5 eV and 529.4 eV, respectively, when compared to CAT A. In addition, other peaks appeared at 534.7 and 535.5 eV for CAT B and CAT C, respectively, which may be related to changes in the chemical composition of the catalysts, linked to the formation of Ce^{3+} on the external surface. The lower intensity of the peak O1s (529.5 eV) and the absence of the signal at 534.7 eV (observed only in the CAT B and CAT C catalysts) can be associated with a lower concentration of Ce^{3+} species at the outer walls of the nanotubes of the CAT A. Here the CeO_2 was deposited on the outer walls of the nanotubes, while for CAT B and CAT C, the cerium oxide was deposited on the inner wall of the CNT. Noteworthy is that the CAT C catalyst presents the most intense O1s band, due to a higher concentration of CeO_2 (7.5 wt.% total), therefore suggesting a higher formation of Ce^{3+} species compared to the other samples. In fact, the higher the formation of Ce^{3+} on the surface, the more vacancies are present. As reported in the literature [46], the oxygen vacancies in ceria lead to higher oxygen mobility and diffusion from lattice to the interface of copper and cerium oxides, and favor the formation of Cu^+ species through the redox equilibrium of $Cu^{2+} \leftrightarrow Cu^+$ and $Ce^{4+} \leftrightarrow Ce^{3+}$.

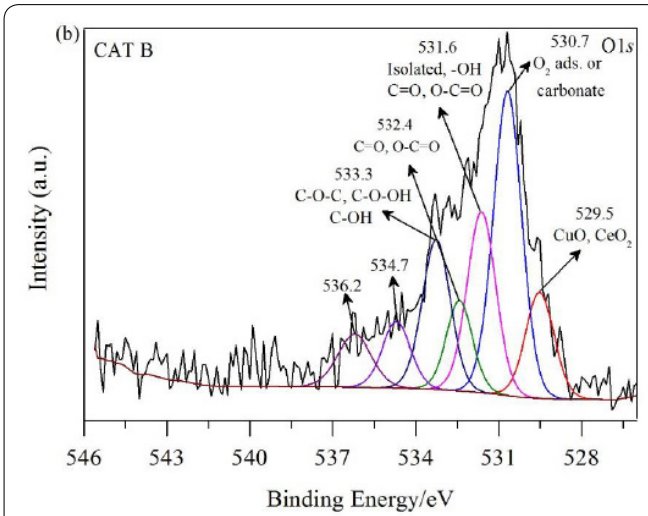

Figure 6: Peak deconvolution O1s of the (b) CuO/CNT@CeO_2 (CAT B) catalyst. The standard C1s line at 283 eV was used as calibration reference. Supplementary material 1: (a) CeO_2/CNT@CuO (CAT A) and (c) CuO-CeO_2/CNT@CeO_2 (CAT C) catalysts.

Figure 7 displays the $Cu_2p1/2$ and $Cu_2p_3/2$ spectra of CAT A (CeO_2/CNT@CuO), CAT B (CuO/CNT@CeO_2), and (CAT C(CuO-CeO_2/CNT@CeO_2). The standard C1s line at 283 eV was used as a calibration reference.

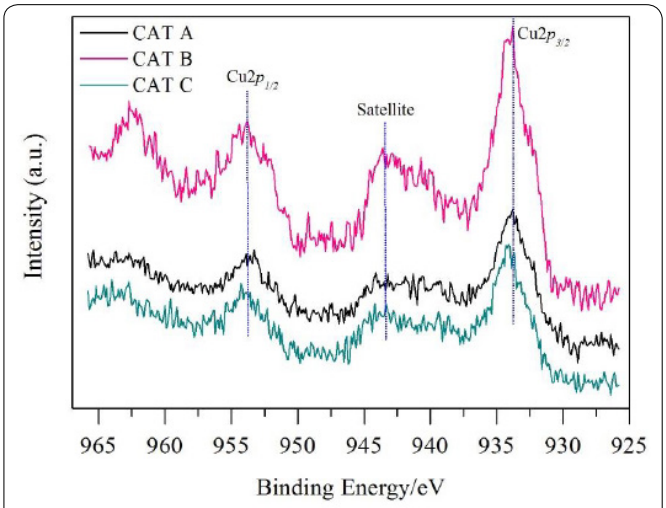

Figure 7: Comparative XPS spectrum for Cu of the CAT A, CAT B and CAT C catalysts.

The peaks at 933.8 and 953.5 eV (CAT A), 933.9 and 953.5 eV (CAT B), 934.1 and 953.7 eV (CAT C), are respectively associated with $Cu2_{p3/2}$ and $Cu2_{p1/2}$ (Figure 7) [47]. Peaks at 933.8 eV for CAT A, 933.9 eV for CAT B, and 934.1 eV for CAT C, and the satellites at 943.2, 943.5 eV and 943.1 eV for CAT A, CAT B and CAT C respectively, demonstrated the predominant formation of Cu^{2+} [$Cu_{2p3/2}$; 932.18 eV for Cu^+ and 933.76 eV for Cu^{2+})] [40, 48, 49]. The binding energy varies slightly among the catalysts. In fact, it is possible that Cu^+ is present [50]. The small differences observed in binding energy (0.1 to 0.5 eV) are in the standard deviation [61].

Supplementary material 1 displays the deconvolution of Cu $2p_{3/2}$ spectrum of CAT A (CeO_2/CNT@CuO), CAT

B ($CuO/CNT@CeO_2$), and CAT C ($CuO\text{-}CeO_2/CNT@CeO_2$). The standard C1s line at 283 eV was used as a calibration reference. The small differences in binding energy (0.1 to 0.3 eV) may be related to small changes in copper and/or cerium electronegativity, possibly produced by the formation of various types of chemical bonds, associated with Cu^{2+}, Cu^{1+}, Ce^{3+} species. In this sense, the presence of these species can influence the electrochemical properties of the oxygen network.

Supplementary material 1 displays the deconvolution of Ce_3d spectrum for CAT A ($CeO_2/CNT@CuO$), CAT B ($CuO/CNT@CeO_2$), and CAT C ($CuO\text{-}CeO_2/CNT@CeO_2$).

The XPS spectra also showed $Ce3d_{3/2}$ and $Ce3d_{5/2}$ peaks due to the presence of CeO_2, representing the combination of the 4f atomic orbitals of the cerium and 2p atomic orbitals of the oxygen (Supplementary material 1). The peaks at 916.5, 906.5, 903.6 and 900.9 eV for CAT A; 916.5, 906.3, 903.9 and 900.5 eV for CAT B; and 916.4, 906.5, 903.3 and 900.8 eV for CAT C represent the functions u'", u", u', u of the $Ce_3d_{3/2}$, respectively. The functions v'", v", v', v which represent the $Ce3d_{5/2}$ peaks were observed at 898.6, 888.6, 885.1 and 882.3 eV (CAT A); 897.8, 887.8, 884.9 and 881.8 eV (CAT B); and 897.9, 888.2 886.1 and 882.0 eV (CAT C). Photoemission of Ce^{4+} was observed in the u'"/v'" functions. The reduced and formed species by the transfer of one or two electrons from the full O2p orbital to a partially full Ce4f orbital are represented by the u/v and u"/v" functions [51, 52]. The u' and v' functions are characteristic of Ce^{3+} cations formed from the interaction between cerium and surrounding atoms [53]. Also, it may be related to oxygen vacancies resulted from incomplete oxidation of CeO_2 (111). The binding energies have changed somewhat between catalysts (< 0.5 eV).

Figure 8 shows peaks referring to cerium, which are more intense for CAT B (5% internal CeO_2), followed by CAT A (5% external CeO_2). This feature is in accordance with the chemical composition of the catalysts. The concentration of cerium for CAT C catalyst is low as expected because only 2.5% of cerium oxide was deposited on the outer surface and the remaining 5% was deposited on the inner walls. This feature is represented by figure 8. In contrast, the peaks associated with copper, as shown in figure 7, are more in intense for CAT B, followed by CAT C and CAT A. These observations can be used as an indirect measure of selectivity achieved during the synthesis.

Table 2 shows the values of the relative concentration of Ce and Cu on the surface of the catalysts estimated by XPS. The concentration of Ce and Cu species was lower than expected. The difference observed may be related to the limited pore effect. The detection depth is limited by the photoelectron (< 2 nm). Thus, nanoparticles deposited in the mesoporous are not accurately quantified. Also, the walls of the nanotubes interfere with the signal, and therefore less intense peaks are observed.

Table 2: Relative concentration of the species detected in the XPS spectra of the catalysts.

Catalyst	C1s	O1s	Cu_2p	Ce_3p
CAT A	92.4	6.87	0.53	0.22
CAT B	93.6	5.07	1.01	0.31
CAT C	93.8	5.26	0.53	0.38

On the other hand, it was observed that the concentration of Ce and Cu is not proportional to the relative concentration of the metal oxides that have been deposited on the outer and inner surface of the nanotubes. The external concentrations of Ce and Cu for CAT C are similar (2.5% CuO and 2.5% CeO_2), however, the relative surface concentrations are low.

TPR analyses

The samples were pretreated with He under a flow rate of 60 $mL.min^{-1}$ for 1 h at 450 °C and heating rate of 10 $°C.min^{-1}$. Thereafter, the samples were cooled down to room temperature under helium flow and finally reduced with 10% H_2/Ar (60 $mL.min^{-1}$) at 10 $°C.min^{-1}$ up to 650 °C. The hydrogen signal was followed and monitored by a mass spectrometer. The TPR profiles are shown in figure 9.

The reduction profiles of the catalysts display several peaks. For CAT A sample there are three main peaks (α, β and

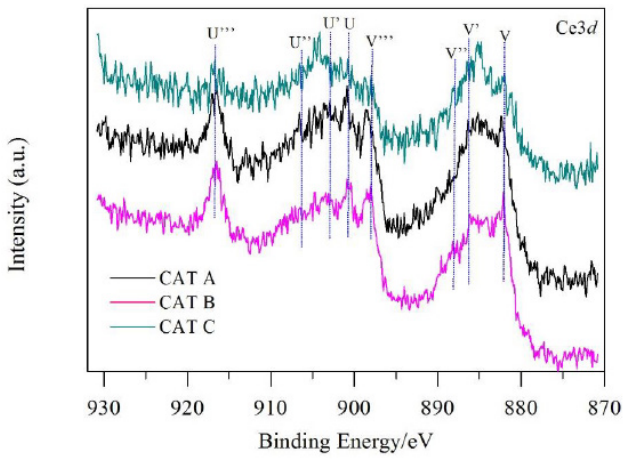

Figure 8: Comparative XPS spectrum for Ce of the CAT A, CAT B and CAT C catalysts.

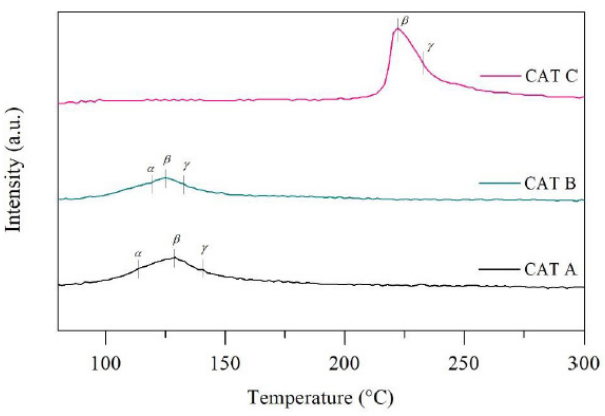

Figure 9: TPR-H_2 of the functionalized (CNTF), raw material (CNT) and catalysts: $CeO_2/CNT@CuO$ (CAT A), $CuO/CNT@CeO_2$ (CAT B) e $CuO\text{-}CeO_2/CNT@CeO_2$ (CAT C).

γ) between 110 and 145 ˚C. Peak α (112 ˚C) was attributed to the reduction of CuO nanoparticles. On the other hand, the β (128 ˚C) and γ (142 ˚C) peaks are related, respectively, to the CuO species and the reduction of bulk CuO [11, 53]. These results suggest that the Cu precursor is dispersed on the inner surface of the catalyst (CAT A) interacting with the inner surface of the nanotubes which favored the reduction of CuO at lower temperatures. CAT B exhibited similar profiles and that suggests only the reduction of CuO at the external wall. It also indicates that the CeO_2 on the inner surface of the nanotubes was not reduced, indicating strong interaction with the internal wall. The profile of CAT C, for which both CuO and CeO_2 oxides are located at the external surface wall and CeO_2 also internally, indicated reduction at higher temperatures than CAT A and CAT B, respectively, at 222 and 248 ˚C. In fact, the β and γ peaks shifted to higher temperatures, indicating that the CuO is influenced by the presence of CeO_2. For CAT C the β peak is more intense than on CAT A and CAT B, and the presence of CeO_2 difficult their reduction, suggesting reduction of isolated CuO and partial interaction with CeO_2 which is mostly associated with the reduction of superficial ceria, as observed by XPS. Therefore, the presence of Ce^{3+} on CAT C suggests that reduced Cu species may facilitate the reduction of CeO_2 on the external surface. The CeO_2 in the form of Ce^{3+} ions, improved the formation of vacancies. Noteworthy is that isolated CeO_2 particles are not reduced, located internally or externally on the CNT walls. The conclusion is that CAT A and CAT B evidenced the presence of isolated metal oxides, and CAT C evidenced low surface interaction of CuO with CeO_2 on the external surface.

PROX Reaction

The samples were pretreated with He, at a flow rate of 60 $mL.min^{-1}$ for 1 h, at 450 ˚C and heating rate of 10 ˚C.min^{-1}. Thereafter the samples were cooled down to room temperature under helium flow. Then, the samples were reduced with 10% H_2/Ar (60 $mL.min^{-1}$) at 10 ˚C.min^{-1} up to 450 ˚C. The CO oxidation was performed at different temperatures. The support itself is not active for this reaction under such conditions, in accordance with the references [11] and [24]. The CO conversions at 150 ˚C were similar around 30% for the three catalysts. At 180 ˚C the conversions obtained for CAT A and CAT B were of the order of 56% and reached maximum conversions of 57% for 200 ˚C, which suggests that the selective deposition of the metal oxides CuO and CeO_2 on the inner or outer walls does not affect the conversion. For the external bimetallic CAT C (CuO- CeO_2/CNT@CeO_2) the conversion was 51% at 180 and 200 ˚C.

The activity was calculated determining the reaction rates based on the total mass of metallic oxides (10% wt.), as displayed in figure 10.

The rates (per gram of total metal) of CAT A (CeO_2 external) and CAT B (CuO external) are similar and higher than CAT C (CuO + CeO_2 external). Noteworth, the reaction rate increased 2 times when temperature increased from 150 to 180 ˚C, and reached maximum rate at 200 ˚C. The higher

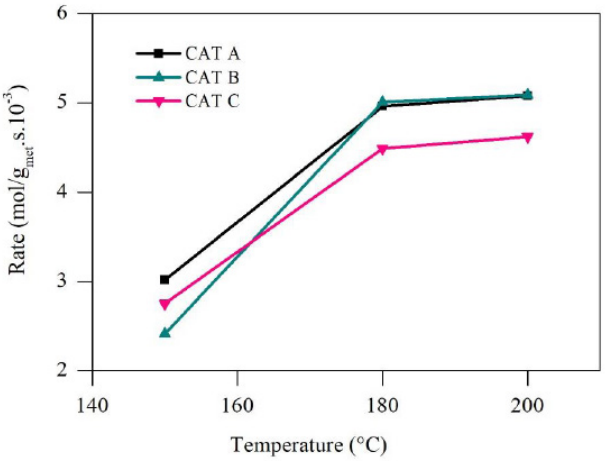

Figure 10: Rate of reaction based on the total mass of metallic oxides, 10% CuO and 10%CeO_2 and CAT C (2.5% CuO and 7.5%CeO_2)

reaction rates of CAT A and CAT B can be attributed to the high particle dispersions of CuO (3.7 nm), and CeO2 (4.8 nm) on CNT in and outer walls, respectively which contributes to the redox processes. However, for the bimetalllic oxide on CAT C, the rate decreases, due to the lower concentration of CuO (2.5%) and CeO_2 (2.5%) on the external walls of the CNTs, compared to CAT A and CAT B, and hence the lower copper dispersion in the presence of ceria oxide on the external CNT wall. Zhu [9] observed that the CuO concentration influenced the activity. Based on these results we can affirm that the activity is independent of the location or selective deposition of metal oxides inside or outside the carbon nanotube walls of CAT A and CAT B, but depends on the CuO and CeO_2 concentration (CAT C). In fact, the CNT facilitates the dispersion of metal oxide inside or outside the CNT walls and the activity is independent of their location.

The CO_2 selectivity decreases as the temperature increases. High selectivity (100%) was achieved at 150 ˚C for CAT A catalyst and high O_2 conversion (100%) was reached between 180 and 200 ˚C, besides the formation of water. In fact, oxidation of H_2 occurs with increasing temperature on CuO, besides the reverse water-gas shift reaction [56]. Noteworthy is that methane was not observed, indicating that under such conditions the methanation reaction does not occurr. The bimetallic catalyst CAT C showed lower selectivity than CAT A and CAT B, as shown in figure 11, which can be assigned to the lower concentrations of the metal oxides on the external CNT walls and thus their dispersions.

Stability

The stability tests were carried out isothermally at 180 ˚C for all catalysts. After pretreatment and reduction in H_2, the catalytic bed was cooled down and set at the test temperature. Tests were performed under space velocity of 60.000 $mL.g^{-1}.min^{-1}$ for 20 h. The results are shown in figure 12.

Figure 12 shows excellent stability over time (20 h). In addition, supplementary material 2 presents CO_2 selectivity. The catalysts reached high conversions 65-70%. It demonstrates that the catalysts are stable under the reaction conditions.

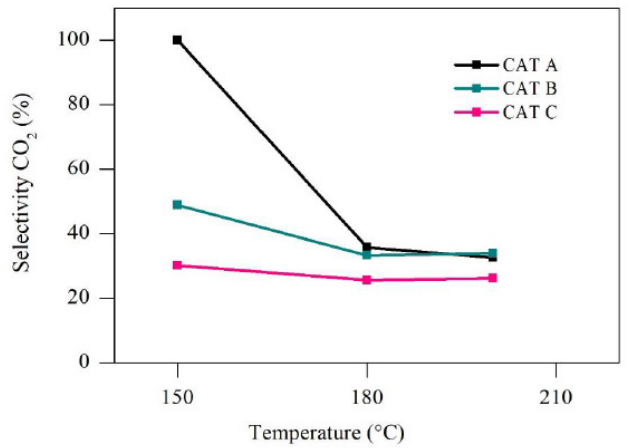

Figure 11: CO_2 selectivity tests for CeO_2/CNT@CuO (CAT A), CuO/CNT@CeO_2 (CAT B) and CuO-CeO_2/CNT@CeO_2 (CAT C), Test conditions: 2% CO, 2% O2, 54.7% H2.

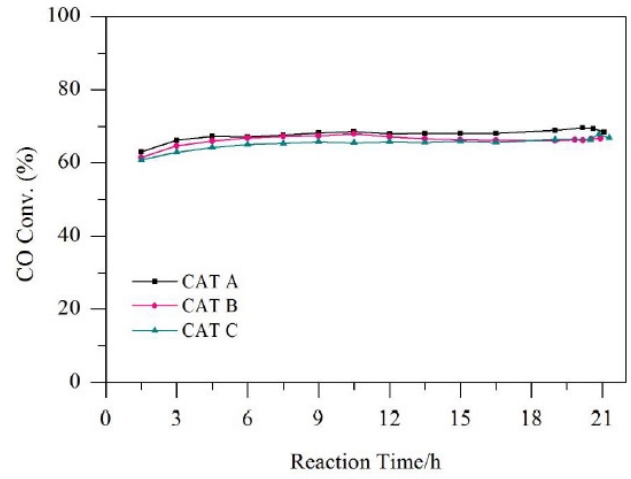

Figure 12: Stability tests for CeO_2/CNT@CuO (CAT A), CuO/CNT@CeO_2 (CAT B) and CuO-CeO_2/CNT@CeO_2 (CAT C). CO conversions at 180°C. Reaction for 20 h.

Electronic effects

Since the nanotubes provide a high specific area, the dispersion of the oxides increases inside and outside the walls. which favors the dispersion of the active phase on the surface of CNT walls. In fact, the chemical properties of the outer surface of the nanotubes are different compared to the nano-confined space, characteristic of the internal walls of CNTs. Catalysts CAT A, CAT B, CAT C indicate isolated and dispersed metal oxides over the internal and external walls, and not the formation of a solid solution, in opposition to Shi [11] for mixed oxides $Cu_xCe_{1-x}O$/CNTs catalysts.

On the other hand, the XPS results also showed the presence of Cu^+/Cu^{2+} or Ce^{3+}/Ce^{4+} surface species that may favoring the adsorption of molecules and the oxygen storage capacity in their vacancies, essentials for the reaction. Indeed, according to the literature, the metal oxides deposited on the outer walls of the nanotubes suggest that the p orbitals of the carbon atoms increase the adsorption of diatomic molecules (CO and H_2) on metal oxides, and therefore promote the dissociation of molecules and two orbitals of the molecules, since they can occupy the highest levels (HOMO) and the lowest level (LUMO) that allow the adsorption on surfaces of these catalysts [63]. Therefore, the electronic properties of CuO and CeO_2 are modified, benefiting the activity of the catalysts. In addition, the curved surface of the CNT favors also the diffusion of the molecules [39]. Therefore, the activity depends not only on the dispersion but on the electronic properties of the metal oxide or metal ion species over the support and of the CNT support. The CNT favors the electronic mobility of the electrons between the metal oxide and the CNTs and thus its stability.

Post reaction analysis

The MWCNTs are inert, avoid sintering or interactions with the active metal oxides and carbon deposition during the PROX reaction. The main consequence is the structure modification of the CNT and the structure modification of the metal oxides. Therefore, after the stability tests, the catalysts were analyzed by X-ray diffraction. XRD patterns (Figure 13) showed graphite, CeO_2 and CuO phases.

The diffraction peaks at 2Θ = 26° e 78° were associated

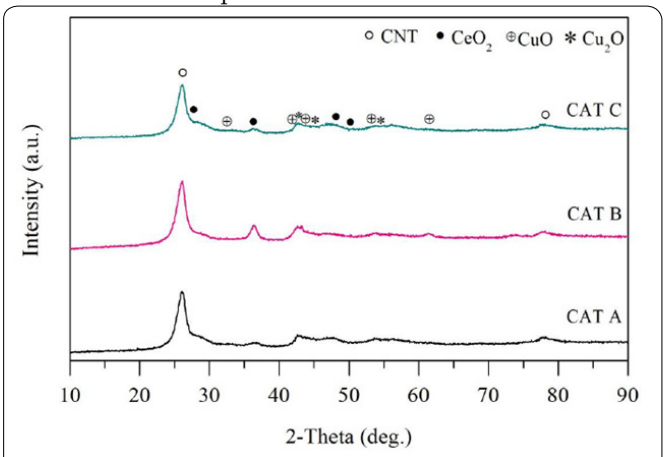

Figure 13: XRD patterns of CeO_2/CNT@CuO (CAT A), CuO/CNT@CeO_2 (CAT B) and CuO-CeO_2/CNT@CeO_2 (CAT C) catalyst after stability test.

with the crystallographic planes (0 0 2) of the graphite layers. This suggests that catalysts are stable, and nanotubes maintain their structural characteristics after 20 h of reaction. The peaks at 2Θ = 32.26°, 42.24°, 44.21°, 53.32° and 61.36° correspond to the CuO phase (PDF#44-0706). The CeO_2 phase was identified at 2Θ = 27.37°, 36.76°, 48.12°, and 50.59° (PDF#44-1001). Also, an additional phase was identified. The peaks at 2Θ = 42.64°, 44.85°, and 53.86° are linked to the Cu_2O phase (PDF#35-1091). The Cu_2O phase confirms the reduction of the copper during the catalytic reaction, as expected. CuO phase became more intense in the CAT A catalyst, whereas the intensity of the CeO_2 phase was very similar for both catalysts (CAT A and CAT B). The diffraction pattern of the CAT C catalyst showed that the peaks of the CuO phase are less intense compared to the peaks shown by the CAT A and CAT B catalysts. No sintering or interaction of CuO-CeO_2 were observed, contrary to the results observed for these metal oxides on the mexed oxides supports.

Conclusion

CuO and CeO_2 catalysts were synthesized and supported on multiple-walled carbon nanotubes. Metallic oxides were selectively deposited by wet impregnation. Functionalization of the carbon nanotubes led to the oxidation of the ends and lateral walls of this support leaving the inner surface exposed. Structural characterization by XRD showed characteristic peaks of CuO and CeO_2. TEM images showed open ends and the formation of defects on the support surface. Nanoparticles with a mean diameter of 3.7-7.2 nm were associated with CeO_2, whereas nanoparticles with mean diameter of 4.8-5.6 nm were linked to CuO.

The CeO_2/CNT@CuO (CAT A) and CuO/CNT@CeO_2 (CAT B) showed a higher catalytic activity within the temperature range of 180-200 °C than bimetallic CuO- CeO_2/CNT@CeO_2 (CAT C). The CNT facilitates the dispersion of metal oxide inside or outside the CNT walls and the activity are independent of their location. The CO_2 selectivity decreases with the temperature. The selectivity of CAT A catalyst was 100% at 150 °C and O_2 conversion 100% at 180 °C with the formation of water. The bimetallic catalyst CAT C presented lower selectivity due to the lower concentrations of the metal oxides on the external CNT walls.

The catalysts reached high conversions 65-70% and are very stable for long time. The CNT contribute to the electronic mobility of the electrons of metal oxide and the CNTs. There is no sintering or interaction between metal oxides.

Synopsis

Inner empty surface of the MWCNT present different properties that can be used in the synthesis of catalysts. Depositing particles selectively on the inner and/or outer surface of MWCNT is a challenge. Catalysts synthesized according to these parameters have different characteristics. In our work, we demonstrated that it was reached a good selectivity during deposition of the metallic oxides. The materials showed catalytic activity for CO oxidation.

Acknowledgements

The authors would like to acknowledge the High Resolution Electron Microscopy Laboratory (LaMAR) of Fluminense Federal University for the support in TEM analyses. Dayana thanks FAPERJ for the scholarship.

References

1. Lunsford JH. 2000. Catalytic conversion of methane to more useful chemicals and fuels: a challenge for the 21st century. *Catal Today* 63(2-4): 165-174. https://doi.org/10.1016/S0920-5861(00)00456-9
2. Song C. 2002. Fuel processing for low-temperature and high-temperature fuel cells: challenges, and opportunities for sustainable development in the 21st century. *Catal Today* 77(1-2): 17-49. https://doi.org/10.1016/S0920-5861(02)00231-6
3. Roh HS, Potdar HS, Jun KW, Han SY, Kim JW. 2004. Low temperature selective CO oxidation in excess of H_2 over Pt/Ce—ZrO_2 catalysts. *Catalysis Letters* 93: 203–207. https://doi.org/10.1023/B:CATL.0000017077.38760.1f
4. Tanaka H, Ito SI, Kameoka S, Tomishige K, Kunimori K. 2003. Promoting effect of potassium in selective oxidation of CO in hydrogen-rich stream on Rh catalysts. *Catal Commun* 4(1): 1-4. https://doi.org/10.1016/S1566-7367(02)00229-7
5. Wootsch A, Descorme C, Duprez D. 2004. Preferential oxidation of carbon monoxide in the presence of hydrogen (PROX) over ceria–zirconia and alumina-supported Pt catalysts. *J Catal* 225(2): 259-266. https://doi.org/10.1016/j.jcat.2004.04.017
6. Son IH, Lane AM. 2001. Promotion of Pt/γ-Al_2O_3 by Ce for Preferential Oxidation of CO in H_2. *Catalysis Letters* 76: 151-154. https://link.springer.com/article/10.1023%2FA%3A1012293311973
7. Zou H, Chen S, Liu Z, Lin W. 2009. DRIFTS study of Cu–Zr–Ce–O catalysts for selective CO oxidation. *Int J Hydrogen Energ* 34(23): 9324-9333. https://doi.org/10.1016/j.ijhydene.2009.09.060
8. Arias AM, García MF, Gálveza O, Coronado JM, Anderson JA, et al. 2000. Comparative study on redox properties and catalytic behavior for CO oxidation of CuO/CeO_2 and CuO/$ZrCeO_4$ catalysts. *J Catal* 195(1): 207-216. https://doi.org/10.1006/jcat.2000.2981
9. Zhu P, Li J, Zuo S, Zhou R. 2008. Preferential oxidation properties of CO in excess hydrogen over CuO-CeO_2 catalyst prepared by hydrothermal method. *Appl Surf Sci* 255(5 Pt-2): 2903-2909. https://doi.org/10.1016/j.apsusc.2008.08.033
10. Marbán G, Fuertes AB. 2005. Highly active and selective CuO_x/CeO_2 catalyst prepared by a single-step citrate method for preferential oxidation of carbon monoxide. *Appl Catal B-Environ* 57(1): 43-53. https://doi.org/10.1016/j.apcatb.2004.10.011
11. Shi L, Zhang G, Wang Y. 2018. Tailoring catalytic performance of carbon nanotubes confined CuO-CeO_2 catalysts for CO preferential oxidation. *Int J Hydrogen Energ* 43: 18211-18219. https://doi.org/10.1016/j.ijhydene.2018.08.020
12. Zeng S, Zhang L, Jiang N, Gao M, Zhao X, et al. 2015. Multi-wall carbon nanotubes as support of copper–cerium composite for preferential oxidation of carbon monoxide. *J Power Sources* 293: 1016-1023. https://doi.org/10.1016/j.jpowsour.2015.04.115
13. Dongil AB, Baeza BB, Castillejos E, Escalona N, Guerrero Ruiz AG, et al. 2018. Promoter effect of alkalis on CuO/CeO_2/carbon nanotubes systems for the PROx reaction. *Catal Today* 301: 141-146. https://doi.org/10.1016/j.cattod.2017.03.033
14. Dongil AB, Baeza BB, Castillejos E, Escalona N, Ruiz AG, et al. The promoter effect of potassium in CuO/CeO_2 systems supported on carbon nanotubes and graphene for the CO-PROX reaction. *Catal Sci Technol* 6: 6118-6127. https://doi.org/10.1039/C6CY00304D
15. Gao Y, Xie K, Wang W, Mi S, Liu N, et al. 2015. Structural features and catalytic performance in CO preferential oxidation of CuO–CeO_2 supported on multi-walled carbon nanotubes. *Catal Sci Technol* 5: 1568-1579. https://doi.org/10.1039/C4CY01220H
16. Wang X, Li N, Pfefferle LD, Haller GL. 2013. Metal nanoparticles inside multi-walled carbon nanotubes: A simple method of preparation and of microscopic image analysis. *Micropor Mesopor Mat* 176: 139-144. https://doi.org/10.1016/j.micromeso.2013.04.002
17. Tessonnier JP, Ersen O, Weinberg G, Huu CP, Su DS, et al. 2009. Selective deposition of metal nanoparticles inside or outside multiwalled carbon nanotubes. *ACS Nano* 3(8): 2081-2089. https://pubs.acs.org/doi/10.1021/nn900647q
18. Astinchap B, Moradian R, Ardu A, Cannas C, Varvaro G, Capobianchi A. 2012. Bifunctional FePt@MWCNTs/Ru Nanoarchitectures: Synthesis and Characterization. *Chem Mater* 24(17): 3393–3400. https://doi.org/10.1021/cm3015447
19. Ma Q, Wang D, Wu M, Zhao T, Yoneyama Y, et al. 2013. Effect of catalytic site position: Nickel nanocatalyst selectively loaded inside or outside carbon nanotubes for methane dry reforming. *Fuel* 108: 430-438. https://doi.org/10.1016/j.fuel.2012.12.028
20. Figueira CE, Moreira PF, Giudici R, Brito RM, Schmal M. 2018.

Nanoparticles of Ce, Sr, Co in and out the multi-walled carbon nanotubes applied for dry reforming of methane. *Appl Catal A Gen* 550: 297-307. https://doi.org/10.1016/j.apcata.2017.11.019

21. Li W, Liang C, Zhou W, Qiu J, Zhou, et al. 2003. Preparation and characterization of multiwalled carbon nanotube-supported platinum for cathode catalysts of direct methanol fuel cells. *J Phys Chem B* 107(26): 6292-6299. https://doi.org/10.1021/jp022505c
22. Nishikiori H, Tanigaki T, Endo M, Fujii T. 2014. Quantitative characterization of acidic groups on acid-treated multi-walled carbon nanotubes using 1-aminopyrene as a fluorescent probe. *Carbon* 66: 560-566. https://doi.org/10.1016/j.carbon.2013.09.038
23. Zhao F, Gong M, Zhang G, Li J. 2015. Effect of the loading content of CuO on the activity and structure of CuO/Ce-Mn-O catalysts for CO oxidation. *J Rare Earth* 33: 604-610. https://doi.org/10.1016/S1002-0721(14)60460-9
24. Zhang D, Mai H, Huang L, Shi L. 2010. Pyridine-thermal synthesis and high catalytic activity of CeO_2/CuO/CNT nanocomposites. *Appl Surf Sci* 256(22): 6795-6800. https://doi.org/10.1016/j.apsusc.2010.04.091
25. Belin T, Epron F. 2005. Characterization methods of carbon nanotubes: a review. *Mat Sci Eng B Adv* 119(2): 105-118. https://doi.org/10.1016/j.mseb.2005.02.046
26. Behler K, Osswald S, Ye H, Dimovski S, Gogotsi Y. 2006. Effect of thermal treatment on the structure of multi-walled carbon nanotubes. *J Nanopart Res* 8: 615-625. https://doi.org/10.1007/s11051-006-9113-6
27. Scheibe B, Palen EB, Kalenczuk RJ. 2010. Oxidation and reduction of multiwalled carbon nanotubes — preparation and characterization. *Mater Charact* 61(2): 185-191. https://doi.org/10.1016/j.matchar.2009.11.008
28. Polychronopoulou K, Zedan AF, Katsiotis MS, Baker MA, AlKhoori AA, et al. 2017. Rapid microwave assisted sol-gel synthesis of CeO_2 and CexSm1-xO_2 nanoparticle catalysts for CO oxidation. *Molecular Catalysis* 428: 41-55. https://doi.org/10.1016/j.molcata.2016.11.039
29. Polychronopoulou K, Zedan AF, AlKetbi M, Stephen S, Ather M, et al. 2018. Tailoring the efficiency of an active catalyst for CO abatement through oxidation reaction: The case study of samarium-doped ceria. *J Environ Chem Eng* 6(1): 266-280. https://doi.org/10.1016/j.jece.2017.12.001
30. Zedan AF, Polychronopoulou K, Asif A, AlQaradawi SY, AlJaber AS. 2018. Cu-Ce-O catalyst revisited for exceptional activity at low temperature CO oxidation reaction. *Surf Coat Tech* 354: 313-323. https://doi.org/10.1016/j.surfcoat.2018.09.035
31. Osorio AG, Silveira CL, Bueno VL, Bergmann CP. 2008. H_2SO_4/HNO_3/HCl—Functionalization and its effect on dispersion of carbon nanotubes in aqueous media. *Appl Surf Sci* 255(5 Part 1): 2485-2489. https://doi.org/10.1016/j.apsusc.2008.07.144
32. Datsyuk V, Kalyva M, Papagelis K, Parthenios J, Tasis D, et al. 2008. Chemical oxidation of multiwalled carbon nanotubes. *Carbon* 46(6): 833-840. https://doi.org/10.1016/j.carbon.2008.02.012
33. Motchelaho MA, Xiong H, Moyo M, Jewell LL, Coville NJ. 2011. Effect of acid treatment on the surface of multiwalled carbon nanotubes prepared from Fe–Co supported on $CaCO_3$: Correlation with Fischer–Tropsch catalyst activity. *J Mol Catal A Chem* 335(1-2): 189-198. https://doi.org/10.1016/j.molcata.2010.11.033 '
34. Rodríguez-Manzo JA, Cretu O, Banhart F. 2010. Trapping of metal atoms in vacancies of carbon nanotubes and graphene. *ACS Nano* 4(6): 3422-3428. https://doi.org/10.1021/nn100356q
35. Song S, Jiang S. 2012. Selective catalytic oxidation of ammonia to nitrogen over CuO/CNTs: The promoting effect of the defects of CNTs on the catalytic activity and selectivity. *Appl Catal B* 117–118: 346-350. https://doi.org/10.1016/j.apcatb.2012.01.030
36. Kundakovic L, Stephanopoulos MF. 1998. Reduction characteristics of copper oxide in cerium and zirconium oxide systems. *Appl Catal A Gen* 171(1): 13-29. https://doi.org/10.1016/S0926-860X(98)00056-8
37. Iriondo A, Barrio VL, Cambra JF, Arias PL, Guemez MB, et al. 2010. Glycerol steam reforming over Ni catalysts supported on ceria and ceria-promoted alumina. *Int J Hydrogen Energ* 35(20): 11622-11633. https://doi.org/10.1016/j.ijhydene.2010.05.105
38. Zhu H, Wang W, Ran R, Shao Z. 2013. A new nickel–ceria composite for direct-methane solid oxide fuel cells. *Int J Hydrog Energy* 38(9): 3741-3749. https://doi.org/10.1016/j.ijhydene.2013.01.032
39. Qin W, Li X. 2011. A theoretical study on the catalytic effect of nanoparticle confined in carbon nanotube. *Chem Phy Lett* 502(1-3): 96-100. https://doi.org/10.1016/j.cplett.2010.12.030
40. Son IH, Lane AM. 2001. Promotion of Pt/γ-Al_2O_3 by Ce for preferential oxidation of CO in H_2. *Catalysis Letters* 76: 151-154. https://doi.org/10.1023/A:1012293311973
41. Ago H, Kugler T, Cacialli F, Salaneck WR, Shaffer MSP, et al. 1999. Work functions and surface functional groups of multiwall carbon nanotubes. *J Phys Chem B* 103(38): 8116-8121. https://doi.org/10.1021/jp991659y
42. Datsyuk V, Piecourt CG, Dagreou S, Billon L, Dupin JC, et al. 2005. Double walled carbon nanotube/polymer composites via in-situ nitroxide mediated polymerisation of amphiphilic block copolymers. *Carbon* 43(4): 873-876.
43. Zhang X, Cao A, Wei B, Li Y, Wei J, et al. 2002. Rapid growth of well-aligned carbon nanotube arrays. *Chem Phys Lett* 362(3-4): 285-290. https://doi.org/10.1016/S0009-2614(02)01025-4
44. Watts JF. 1993. High resolution XPS of organic polymers. *Surface and Interface Analysis* 20(3): 267. https://doi.org/10.1002/sia.740200310
45. Sun S, Mao D, Yu J, Yang Z, Lu G, et al. 2015. Low-temperature CO oxidation on CuO/CeO_2 catalysts: the significant effect of copper precursor and calcination temperature. *Catal Sci Technol* 5: 3166-3181. https://doi.org/10.1039/C5CY00124B
46. Konsolakis M, Sgourakis M, Carabineiro SA. 2015. Surface and redox properties of cobalt–ceria binary oxides: On the effect of Co content and pretreatment conditions. *Appl Surf Sci* 341: 48-54. https://doi.org/10.1016/j.apsusc.2015.02.188
47. Gopiraman M, Babu SG, Khatri Z, Kai W, Kim YA, et al. 2013. An efficient, reusable copper-oxide/carbon-nanotube catalyst for N-arylation of imidazole. *Carbon* 62: 135-148. https://doi.org/10.1016/j.carbon.2013.06.005
48. Li Y, Su J, Ma J, Yu F, Chen J, et al. 2015. Novel straight synthesis of super-microporous Cu/Al_2O_3 catalyst with high CH_4-SCR-NO activity. *Catal Commun* 65: 6-9. https://doi.org/10.1016/j.catcom.2015.02.020
49. Studt F, Behrens M, Kunkes EL, Thomas N, Zander S, et al. 2015. The mechanism of CO and CO_2 hydrogenation to methanol over Cu-Based catalysts. *ChemCatChem* 7: 1105-1111. https://doi.org/10.1002/cctc.201500123
50. Mrabet D, Abassi A, Cherizol R, Do TO. 2012. One-pot solvothermal synthesis of mixed Cu-Ce-Ox nanocatalysts and their catalytic activity for low temperature CO oxidation. *Appl Catal A Gen* 447-448: 60-66. https://doi.org/10.1016/j.apcata.2012.09.005
51. Wong GS, Vohs JM. 2002. An XPS study of the growth and electronic structure of vanadia films supported on CeO_2(1 1 1). *Surf Sci* 498: 266-274. https://doi.org/10.1016/S0039-6028(01)01761-7
52. Bêche E, Charvin P, Perarnau D, Abanades S, Flamant G. 2008. Ce_3d XPS investigation of cerium oxides and mixed cerium oxide (CexTiyOz). *Surf Interface Anal* 40(3-4): 264-267. https://doi.org/10.1002/sia.2686
53. Liu Y, Liu B, Wang Q, Li C, Hu W, et al. 2012. Three-dimensionally ordered macroporous Au/CeO_2- Co_3O_4 catalysts with mesoporous walls for enhanced CO preferential oxidation in H_2-rich gases. *J Catal* 296: 65-76. https://doi.org/10.1016/j.jcat.2012.09.003
54. Avgouropoulos G, Ioannides T. 2003. Selective CO oxidation over CuO-CeO_2 catalysts prepared via the urea–nitrate combustion method. *Appl Catal A-Gen* 244: 155-167. https://doi.org/10.1016/S0926-860X(02)00558-6

55. Qi L, Yu Q, Dai Y, Tang C, Liu L, et al. 2012. Influence of cerium precursors on the structure and reducibility of mesoporous CuO-CeO_2 catalysts for CO oxidation. *Appl Catal B Environ* 119-120: 308-320. https://doi.org/10.1016/j.apcatb.2012.02.029

56. Zeng S, Liu K, Zhang L, Qin B, Chen T, et al. 2014. Deactivation analyses of CeO_2/CuO catalysts in the preferential oxidation of carbon monoxide. *J Power Sources* 261: 46-54. https://doi.org/10.1016/j.jpowsour.2014.03.043

57. Zeng S, Zhang W, Guo S, Su H. 2012. Inverse rod-like CeO_2 supported on CuO prepared by hydrothermal method for preferential oxidation of carbon monoxide. *Catal Commun* 23: 62-66. https://doi.org/10.1016/j.catcom.2012.02.028

58. Yen H, Seo Y, Kaliaguine S, Kleitz F. 2012. Tailored mesostructured copper/ceria catalysts with enhanced performance for preferential oxidation of CO at low temperature. *Chem Int Ed* 124(48): 12198-12201. https://doi.org/10.1002/ange.201206505

59. Gao Y, Xie K, Wang W, Mi S, Liu N, et al. 2015. Structural features and catalytic performance in CO preferential oxidation of CuO–CeO_2 supported on multi-walled carbon nanotubes. *Catal Sci Technol* 5: 1568-1579. https://doi.org/10.1039/C4CY01220H

60. Kozonoe CE, Brito RM, Schmal M. 2020. Influence of feed rate and testing variables for low-temperature tri-reforming of methane on the Ni@MWCNT/Ce catalyst. *Fuel* 281: 118749. https://doi.org/10.1016/j.fuel.2020.118749

61. Saikova S, Vorobyev S, Likhatski M, Romanchenko A, Erenburg S, et al. 2012. X-ray photoelectron, Cu L_3MM Auger and X-ray absorption spectroscopic studies of Cu nanoparticles produced in aqueous solutions: The effect of sample preparation techniques. *Appl Surf Sci* 258: 8214-8221. https://doi.org/10.1016/j.apsusc.2012.05.024

62. Meng D, Zhan W, Guo Y, Guo Y, Wang L, et al. 2015. A highly effective catalyst of Sm-MnOx for the NH_3-SCR of NOx at low temperature: promotional role of Sm and its catalytic performance. *ACS Catal* 5(10): 5973-5983. https://doi.org/10.1021/acscatal.5b00747

63. Schmal M. 2016. Heterogeneous Catalysis and its Industrial Applications. Springer International Publishing, Switzerland.